

On the presence of metallofullerenes in fullerene-rich circumstellar envelopes

R. BARZAGA,^{1,2} D. A. GARCÍA-HERNÁNDEZ,^{1,2} S. DÍAZ-TENDERO,^{3,4,5} SEYEDABDOLREZA SADJADI,^{6,7} A. MANCHADO,^{1,2,8}
AND M. ALCAMI^{3,4,9}

¹*Instituto de Astrofísica de Canarias, C/ Via Láctea s/n, E-38205 La Laguna, Spain*

²*Departamento de Astrofísica, Universidad de La Laguna (ULL), E-38206 La Laguna, Spain*

³*Departamento de Química, Módulo 13, Universidad Autónoma de Madrid, 28049 Madrid, Spain*

⁴*Institute for Advanced Research in Chemical Science (IAdChem), Universidad Autónoma de Madrid, 28049 Madrid, Spain*

⁵*Condensed Matter Physics Center (IFIMAC), Universidad Autónoma de Madrid, 28049 Madrid, Spain*

⁶*Research Center for Theoretical and Experimental Physics, Chemistry and Space Sciences, Genius Development and ScienceTech Future Co Ltd, Hong Kong (SAR), PR China*

⁷*Laboratory for Space Research, Faculty of Science, Department of Physics, The University of Hong Kong, Hong Kong (SAR), PR China*

⁸*Consejo Superior de Investigaciones Científicas (CSIC), Spain*

⁹*Instituto Madrileño de Estudios Avanzados en Nanociencia (IMDEA-Nano), Campus de Cantoblanco, Madrid 28049, Spain*

ABSTRACT

The presence of neutral C₆₀ fullerenes in circumstellar environments has been firmly established by astronomical observations as well as laboratory experiments and quantum-chemistry calculations. However, the large variations observed in the C₆₀ 17.4 μ m/18.9 μ m band ratios indicate that either additional emitters should contribute to the astronomical IR spectra or there exist unknown physical processes besides thermal and UV excitation. Fullerene-based molecules such as metallofullerenes and fullerene-adducts are natural candidate species as potential additional emitters, but no specific species has been identified to date. Here we report a model based on quantum-chemistry calculations and IR spectra simulation of neutral and charged endo(exo)hedral metallofullerenes, showing that they have a significant contribution to the four strongest IR bands commonly attributed to neutral C₆₀. These simulations may explain the large range of 17.4 μ m/18.9 μ m band ratios observed in very different fullerene-rich circumstellar environments like those around planetary nebulae and chemically peculiar R Coronae Borealis stars. Our proposed model also reveals that the 17.4 μ m/18.9 μ m band ratio in the metallofullerenes simulated IR spectra mainly depends on the metal abundances, ionization level, and endo/exo concentration in the circumstellar envelopes. We conclude that metallofullerenes are potential emitters contributing to the observed IR spectra in fullerene-rich circumstellar envelopes. Our simulated IR spectra indicate also that the James Webb Space Telescope has the potential to confirm or refute the presence of metallofullerenes (or even other fullerene-based species) in circumstellar environments.

Keywords: astrochemistry — circumstellar matter — infrared: stars — planetary nebulae: general — stars: chemically peculiar

1. INTRODUCTION

The detection of the most common fullerene species (C₆₀) in Planetary Nebulae (PNe) and diverse astrophysical environments have raised the exciting possibility that other more complex fullerene-based molecules

(e.g., metallofullerenes, multishell fullerenes, fullerene-adducts) might be ubiquitous in space and continue to be serious candidates to explain several astrophysical phenomena like the unidentified infrared bands (UIRs), the UV-bump, and the diffuse interstellar bands (DIBs), among others (see Kwok 2016, for a review). This idea was reinforced in 2015 when the fullerene cation (C₆₀⁺) was established as the only DIB carrier known to date (Campbell et al. 2015).

The presence of neutral C_{60} in space is deduced from the detection of its four strongest mid-IR emission bands (those at ~ 7.0 , 8.5 , 17.4 , and $18.9 \mu\text{m}$)¹. The neutral C_{60} mid-IR bands have been (mainly) detected in the circumstellar environments of young PNe (e.g., Cami et al. 2010; García-Hernández et al. 2010) but also in other types of circumstellar environments like those around R Coronae Borealis (RCB) stars (García-Hernández et al. 2011a).

Recent experimental studies combined with quantum-chemical calculations demonstrate also that fullerenes would react with metal atoms and molecules (e.g., polycyclic aromatic hydrocarbons; PAHs), forming a rich family of fullerene-based molecules such as endo(exo)hedral metallofullerenes and fullerene-PAH adducts (e.g., Dunk et al. 2013). These fullerene derivatives may still be excited by UV photons, emitting through the same IR vibrational modes as empty C_{60} cages. For example, laboratory work shows that the strongest mid-IR features of fullerene-PAH adducts are strikingly coincident with those from neutral C_{60} , suggesting that fullerene-based molecules may contribute to the four C_{60} mid-IR features observed in fullerene-containing circumstellar environments (García-Hernández et al. 2013).

In fact, Brieve et al. (2016) recently made a detailed comparison of their laboratory inferred C_{60} emission band strengths with the astrophysical data on fullerene-rich circumstellar environments, showing that the observed strengths cannot be explained in terms of fluorescent or thermal emission alone. They concluded that the C_{60} emission ratios of $17.4\mu\text{m}/18.9\mu\text{m}$ observed imply that they have a contribution of other emitters, or that physical processes other than thermal or UV excitation affect the C_{60} vibrational modes². Here we present a theoretical study based on quantum-chemistry calculations of endo(exo)hedral metallofullerenes (both neutral and charged), showing that they significantly contribute to the four IR bands generally attributed to neutral C_{60} and may explain the large range of the C_{60} $17.4\mu\text{m}/18.9\mu\text{m}$ band ratio observed in very different circumstellar environments like those around PNe and RCB stars. Our simulated IR spectra indicate that the James Webb Space Telescope (JWST) has the potential

to confirm or refute the presence of metallofullerenes in circumstellar environments.

2. COMPUTATIONAL DETAILS

Quantum chemical calculations on the molecular geometry and spectroscopic properties of twenty-eight neutral and charged metallofullerenes have been performed in the framework of Density Functional Theory (DFT). In particular geometry optimization was carried out at the B3LYP/6-31G(d) level (Becke 1993; Lee et al. 1988; Ditchfield et al. 1971) with the Gaussian 16 code (Frisch et al. 2016; Dennington et al. 2019). Accuracy benchmarking of this level of theory has been previously reported (Robledo et al. 2014; Wang et al. 2017). Spin multiplicity ($2S + 1$) has been considered in the calculations to a maximum of $S = 5/2$, according to the metal multiple charged states. The chemical formulas of these species are $[M-C_{60}]^{0/+}$ (exohedral) and $[M@C_{60}]^{0/+}$ (endohedral) where $M = \text{Li, K, Na, Ca, Mg, Fe, Ti}$ ³. All the geometries used has been characterized as local minimum, with non-imaginary frequencies observed. In order to simulate the vibrational spectra of these species the harmonic oscillator approximation was assumed and, subsequently, harmonic frequencies were adjusted applying a double-scaling-factors scheme to account for anharmonicity, vibro-rotational couplings, etc. (Zapata Trujillo & McKemmish 2022). This approach guaranteed an error $< 2\%$ in the calculated frequencies of C_{60} , used as benchmarking system, with respect to the experiments (Kern et al. 2013). The total mixture spectra of the metallofullerenes were modelled by the simple addition of each IR intensity. In all the spectra, the peak intensity has been simulated by a Gaussian function of FWHM $= 5 \text{ cm}^{-1}$, which is similar to the astronomical observations. The throughout procedure here implemented to simulate the intensity, accounting for the metal atoms concentration/abundance, is presented in the Appendix A. The atomic charges were obtained from electron density partitioning described by the Quantum Theory of Atoms in Molecules (QTAIM), employing the AimAll software (Bader 1990; Keith 2019). Total relative energies have been computed with respect to the most stable structure, thus, a zero value represented it.

3. RESULTS AND DISCUSSION

The simulated IR ($\sim 5\text{-}50 \mu\text{m}$) spectra in the next two subsections have been constructed from the total mixture spectrum procedure (Sect. 2). In order to identify the distinctive spectral features of metallofullerenes,

¹ The mid-IR features of the fullerene cation (C_{60}^+) have only been detected in the reflection nebula NGC 7023 (Berné et al. 2013).

² Brieve et al. (2016) also demonstrate that, in contrast to other C_{60} band ratios (e.g., those involving the 7.0 and $8.5 \mu\text{m}$ features), the $17.4\mu\text{m}/18.9\mu\text{m}$ band ratio should remain almost constant independently of the C_{60} excitation model assumed (fluorescence or thermal models).

³ We consider the most abundant metals and/or well known to be present in the interstellar medium.

Figs. 1 and 2 include the four strongest features of C_{60} (Kern et al. 2013; Sadjadi et al. 2022), according to our own calculations (Sect. 2). The blue dashed lines represent the simulated C_{60} features with a height describing the intensity of the corresponding peak. Note that the intensity of the C_{60} features was scaled equally to the amount of metallofullerenes; i.e., assuming that the same amount of C_{60} molecules and metallofullerenes exist. The total weighted spectrum approach, however, is applied in the third subsection; for further details see Appendix A. Further information about the simulated IR spectra for all the metallofullerene species (28) will be publicly available for the astronomical community in a forthcoming paper (Barzaga et al.).

3.1. Exofullerenes

Figure 1 shows the mixture of exofullerenes spectra, neutral and charged separately; C_{60} features (in blue) are also included for comparison. The positions of the strongest features in both neutral and charged exofullerenes are coincident with those of C_{60} ⁴. The neutral metalloexofullerenes $[M-C_{60}]$ exhibit an IR spectrum richer than their charged counterparts; with a broadening and splitting of the IR features, mainly characterized by a modification of their intensity in comparison to C_{60} . Multiple features appear in the 6-9 μm region; specially, the highest intensity peak at 7.34 μm , which overcome the 7.09 μm C_{60} feature. Similarly, above 14 μm , the spectral fingerprint of $[M-C_{60}]$ is the emergence of several IR peaks accompanied with an inversion of the 17.4 μm /18.9 μm band ratio. The diversity of new 6-9 μm IR features in the $[M-C_{60}]$ spectrum reflects the binding of the metal to the C_{60} carbon cage, while the change in the 17.4 μm /18.9 μm ratio (which are the vibrational modes related to the cage stretching) it is likely due to a charge redistribution provoked also by the metal. The C_{60} 17.4 μm /18.9 μm ratio displays values between 0.41 and 0.79, according to experiments and DFT calculations, respectively (Kern et al. 2013; Sadjadi et al. 2022); in our simulations such ratio for C_{60} is 0.40 (blue dashed lines in Figure 1). However, the 17.4 μm /18.9 μm ratio in the $[M-C_{60}]$ mixture spectrum is 1.89 (Fig. 1). Interestingly, the 17.4 μm /18.9 μm ratio is not inverted (0.55) in the charged metalloexofullerene $[M-C_{60}]^+$ mixture spectrum (Fig. 1), which is more characteristic of an electrostatic interaction (Parker 2010; Jaeger et al. 2004; Szczepanski et al. 2006) and non-covalent metal-

C_{60} forces (Robledo et al. 2014); i.e., the lack of new IR features in the 6-9 μm C-C stretching region together with a global spectral resemblance to pristine C_{60} .

3.2. Endofullerenes

The neutral metalloendofullerenes $[M@C_{60}]$ show their most intense feature at 7.32 μm because of the off-centered inclusion of the metal in the C_{60} cage (Fig. 2). Such effect creates a strong asymmetry in the C_{60} because carbon atoms trend to disrupt the cage in order to accommodate the metal. The perturbation of C-C stretching modes by the binding of the metal implies the whole cage instead of a section, like in the case of neutral metalloexofullerenes. This implies an important increment in the intensity of the IR features within the 6-9 μm region in comparison to pure C_{60} (Fig. 2); even surpassing the IR features intensity for the neutral metalloexofullerenes mentioned above (Fig. 1). The strong broadening and splitting of the $[M@C_{60}]$ mixture spectrum in the 6-9 μm region is again an indication of the metal-carbon cage binding⁵. However, above 14 μm the spectral landscape of $[M@C_{60}]$ considerably diminishes; specially the 18.9 μm feature intensity, which results in a 17.4 μm /18.9 μm ratio of 2.55. In the case of charged metalloendofullerenes $[M@C_{60}]^+$ the reduction of the IR features intensity takes place over all the $\sim 5\text{-}50\mu\text{m}$ spectral region; particularly, in the 6-9 μm C-C stretching region. Such intensity reduction likely implies a lack of charge transfer between the metal and C_{60} carbon cage. In spite of this, the 17.4 μm /18.9 μm ratio (0.40) is almost identical to the one for C_{60} .

3.3. Charge vs Neutrality

Both charged and neutral metallofullerenes would co-exist in circumstellar envelopes since one of the reactants in the metallofullerenes formation, the metals, can be already ionized by the central star (e.g. García-Hernández et al. 2012). In any circumstellar environment, however, the metals have a particular abundance, implying that reliable IR spectra simulations should mix both neutral and charged species but including the specific metal abundances. For this, we have constructed the total weighted mixture spectra in very different fullerene-rich circumstellar envelopes like those around PNe and RCB stars (see details in Appendix A). Figure 3a and b show, respectively, total and total weighted mixture spectra for the C_{60} -PNe case; the intensity has been normalized to ease the comparison. We note that the formation

⁴ The only exception is the $\sim 7.0\mu\text{m}$ feature in the neutral exofullerenes, which is not among the strongest IR features. This feature is certainly present, but blended with the other emission components within the 6-9 μm spectral region.

⁵ Similarly to the neutral exofullerenes, the $\sim 7.0\mu\text{m}$ feature (being not among the strongest features) is present but blended with other higher intensity features inside the 6-9 μm spectral region.

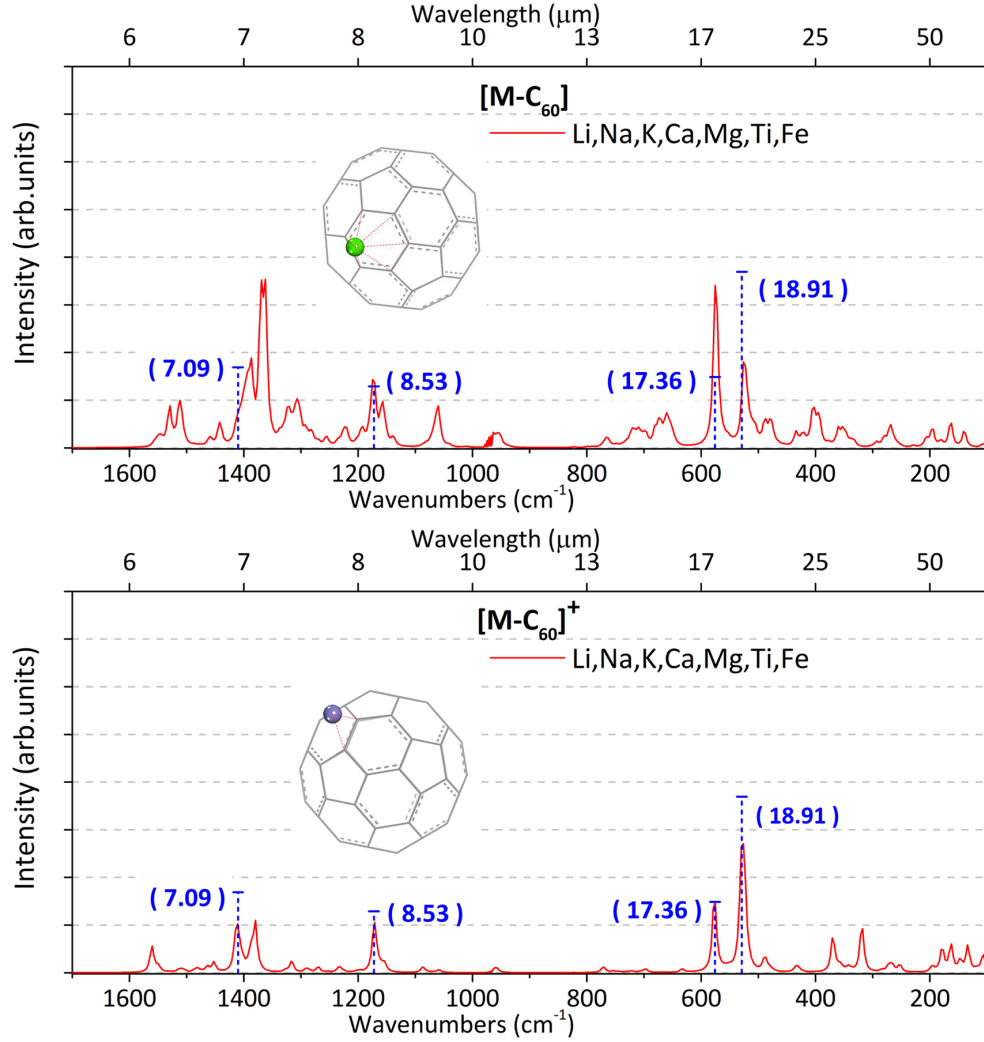


Figure 1. DFT simulated IR ($\sim 5\text{--}50\ \mu\text{m}$) spectra of the mixture of metalloexofullerenes. Top: Seven neutral $[\text{M-C}_{60}]$, Bottom: Seven charged $[\text{M-C}_{60}]^+$. Blue dashed lines represent the features of seven pristine C_{60} molecules, whose intensity is described by the height of the lines. The insets display examples of the most common structures obtained.

probability of endo- versus exo-fullerenes has not been considered because this would require the study of complex kinetic processes, which are out of the scope of this paper. We thus simply assume that both exo- and endo-fullerenes have the same formation probability.

The total mixture spectra has the neutral metallofullerenes as the dominant contributor with an integrated spectral area of 68% (see Fig.3a). Surprisingly, this drastically changes for the total weighted mixture spectra (see Fig.3b), where the neutral metallofullerenes completely dominate the spectrum, with an integrated spectral area of 94%. The metal abundances and ionization fractions expected in C_{60} -PNe circumstellar environments are the two main factors producing such strong modifications in the total weighted mixture spectra. This is because in C_{60} -PNe: i) the metal abundance follows the order, $\text{Mg} > \text{Fe} \gg \text{Na} > \text{Ca} > \text{K} \simeq \text{Ti} > \text{Li}$

(Karakas 2010; Karakas et al. 2018, see Appendix A); and ii) the most abundant metals (Fe, Mg) exhibit the lowest fractions of ionized atoms, around 5-10%; even for the highest effective temperature $T_{\text{eff}} = 50,000\ \text{K}$ observed in C_{60} -PNe (García-Hernández et al. 2012; Otsuka et al. 2014). Indeed, direct thermal effects over the IR intensity can be almost neglected; only very small deviations (a factor of 1.07; see the inset in Fig.3b) are predicted for the narrow T_{eff} range ($\sim 25,000\text{--}50,000\ \text{K}$) of C_{60} -PNe. The noticeable modification of the total weighted mixture spectra prove the importance of the metal abundances and ionization fractions in order to obtain reliable IR simulated spectra. The spectral landscape in Figure 3b is altered in such a way that the $17.4\ \mu\text{m}/18.9\ \mu\text{m}$ ratio varies from 1.21 to 1.03 (total vs total weighted spectra). Thus, our results indicate that

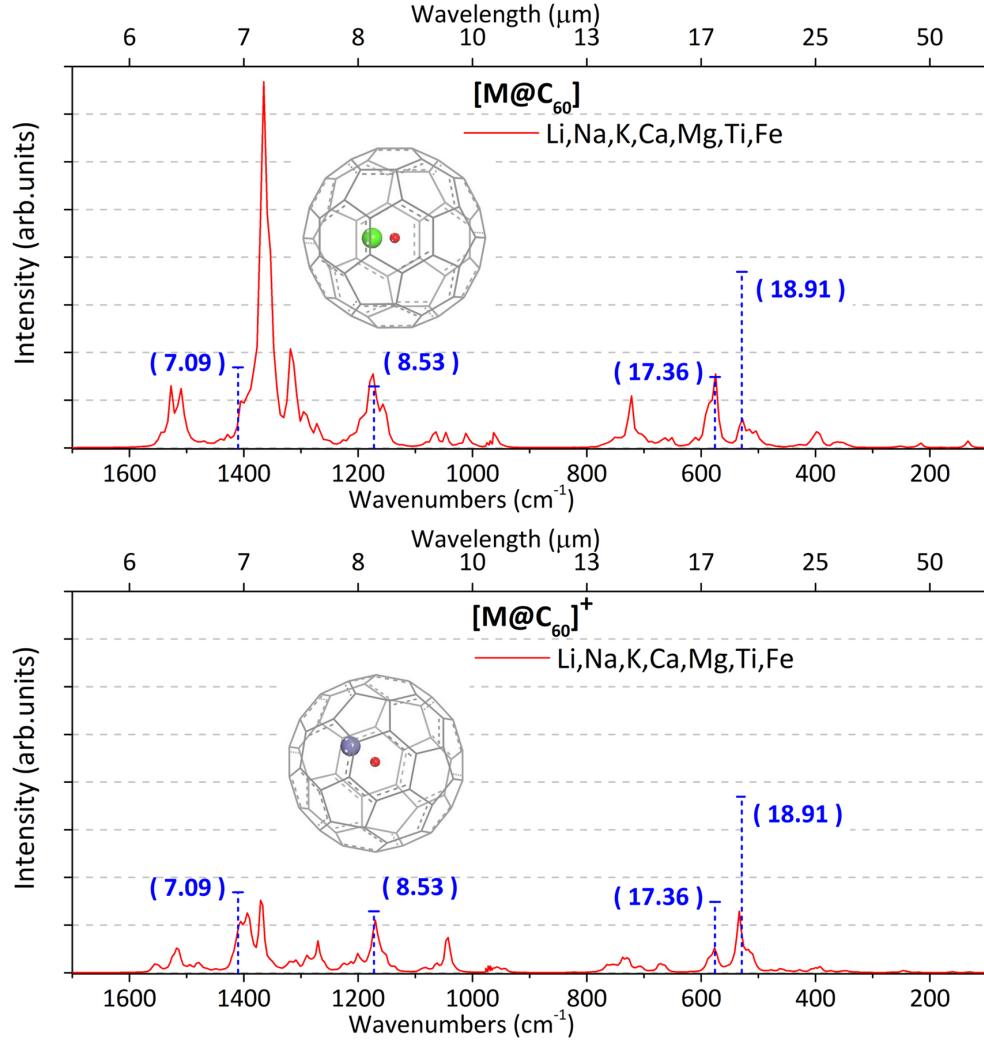
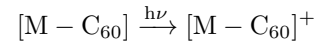
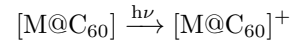


Figure 2. DFT simulated IR ($\sim 5\text{-}50\ \mu\text{m}$) spectra of the mixture of metalloendofullerenes. Top: Seven neutral $[\text{M}@\text{C}_{60}]$, Bottom: Seven charged $[\text{M}@\text{C}_{60}]^+$. Blue dashed lines retain the same description as in Figure 1. The insets display examples of the most common structures obtained but in this case a red dot depicts the centroid of the C_{60} carbon cage.

the $17.4\mu\text{m}/18.9\mu\text{m}$ ratio can be used to track down the presence of charged against neutral metallofullerenes.

Chemical stability is another key factor for the likely preponderance of neutral metallofullerenes. Table 1 displays the relative total energies (E_{tot}^{rel} , see also Sect.2) of all metallofullerenes studied here. Energetically neutral metallofullerenes are the more stable species by an order of $\sim 7\text{ eV}$, which can be attributed to the interaction between the metal and C_{60} , where the charge is compensated. Oppositely, charged metallofullerenes create an uncompensated interaction with the C_{60} cage. Specially for $[\text{M}@\text{C}_{60}]^+$ since the positive charge of the metal is embedded on the carbon cage, which requires more energy to stabilize this charge surrounded by an almost neutral environment. Furthermore, in some cases the C_{60} cage is slightly positively charged hindering even more the energetical stabilization.

On the other hand, once neutral metallofullerenes are formed, charged species can be generated via the photoionization reactions:



Both reactions need to accomplish two requirements: i) photons exciting the neutral metallofullerenes should have energies equal to the corresponding ionization potential; and ii) the production of charged metallofullerenes depends also on the amount of ionizing photons arriving. The first condition, the metallofullerenes ionization potential, can be inferred from the equation $IP = E_{rel}^{total\ charged} - E_{rel}^{total\ neutral}$ using the values

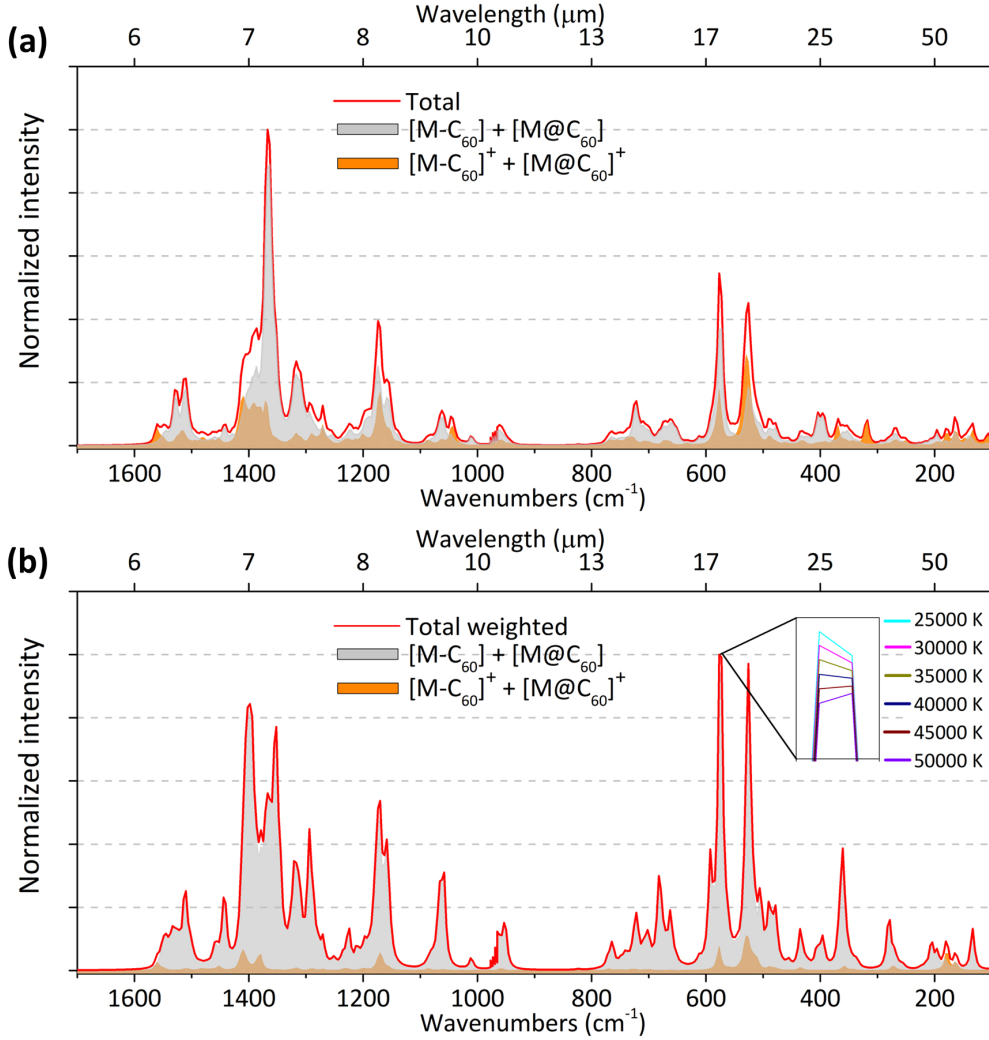


Figure 3. Contributions of neutral and charged metallofullerenes to: (a) Total mixture spectrum from the twenty-eight metallofullerenes. (b) Total weighted spectrum from abundances and ion fraction. Neutral and charged species are denoted by a light-gray and orange filled areas, respectively. An inset highlights the T_{eff} dependent change in the $17.4 \mu\text{m}$ feature intensity for the total weighted spectrum.

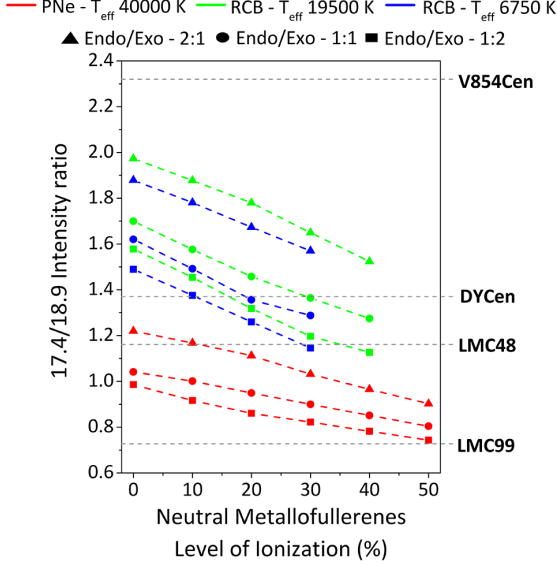
presented in Table 1 between analogous species (e.g., [Ca@C₆₀] vs. [Ca@C₆₀]⁺). This gives a range from ~ 5 to 7 eV, which is an energy easily accessible for the photons emitted by the C₆₀-PNe central stars (CS) (O- and B-type stars; Sternberg et al. 2003). The second condition depends on the flux of ionizing photons leaving the central star, but this flux decays when the central star is cooler (Sternberg et al. 2003). We thus estimate that for a $T_{eff} = 40,000$ K PN central star, a 50% of the ionizing photons would produce charged metallofullerenes, while for the cooler ($< 20,000$ K) RCB stars the flux decays gradually to 10%. Such estimations allow us to observe the effect of charged metallofullerenes overproduction in the $17.4 \mu\text{m}/18.9 \mu\text{m}$ band ratio. Nevertheless, these are rough estimations since for the coolest RCB star V854 Cen ($T_{eff} = 6,750$ K) almost no ionizing photons are

produced according to our black body models. Figure 4 displays the $17.4 \mu\text{m}/18.9 \mu\text{m}$ ratio as a function of the ionization level of neutral metallofullerenes. The data points associated to the curves of RCB stars were calculated according to Appendix A, using the adequate abundances for these stars.

The negative slope observed for the three types of circumstellar envelopes indicate that the $17.4 \mu\text{m}/18.9 \mu\text{m}$ ratio decreases when more charged metallofullerenes are present; i.e., higher ionization level (Fig. 4). The difference between the curves is a direct consequence of the metal abundances, which modify the initial amount of neutral metallofullerenes. Thus, the PNe curves cover a $17.4 \mu\text{m}/18.9 \mu\text{m}$ range of 0.73-1.23, while the RCBs ranges are 1.14-1.88 (V854 Cen) and 1.12-1.97 (DY Cen). Thermal effects mainly imply an increment of

Table 1. Total relative energies in eV (E_{tot}^{rel}) and charge on metal (q^M) and C₆₀ cage ($q^{C_{60}}$).

	[M@C ₆₀]			[M-C ₆₀]			[M@C ₆₀] ⁺			[M-C ₆₀] ⁺		
	E_{tot}^{rel}	q^M	$q^{C_{60}}$	E_{tot}^{rel}	q^M	$q^{C_{60}}$	E_{tot}^{rel}	q^M	$q^{C_{60}}$	E_{tot}^{rel}	q^M	$q^{C_{60}}$
Ca	0	+1.78	-1.78	0.22	+0.91	-0.91	5.54	+1.78	-0.78	5.23	+0.97	+0.03
Mg	0.34	+0.36	-0.36	0	+0.80	-0.80	6.06	+1.09	-0.09	5.34	+0.90	+0.10
Li	0	+0.91	-0.91	0.07	+0.91	-0.91	7.03	+0.91	+0.09	5.12	+0.93	+0.07
Na	0	+0.93	-0.93	0.21	+0.90	-0.90	5.37	+0.89	+0.11	5.04	+0.93	+0.07
K	0	+0.93	-0.93	0.56	+0.91	-0.91	5.36	+0.93	+0.07	5.16	+0.94	+0.06
Fe	1.41	+1.07	-1.07	0	+0.41	-0.41	6.89	+1.04	-0.04	5.61	+0.93	+0.07
Ti	0	+1.36	-1.36	0.46	+0.92	-0.92	5.88	+1.35	-0.35	5.89	+1.21	-0.21

**Figure 4.** The 17.4 μ m/18.9 μ m ratio vs neutral metallofullerenes level of ionization. The several colors and symbols correspond to different circumstellar envelopes (PNe and RCB) and exo/endo fullerenes concentrations, respectively (see legend). The horizontal dashed lines indicate the 17.4 μ m/18.9 μ m ratios observed in two C₆₀-PNe (LMC 48, LMC 99; [García-Hernández et al. 2012](#)), C₆₀-RCBs V854 Cen, DY Cen (this work; [García-Hernández et al. 2011a](#)).

the ionization level although we actually cannot discard possible temperature effects on the kinetics of metallofullerenes formation. Strictly, temperature effects could be important in the transformation of endo- to exo-fullerenes (or viceversa) but such study will be the subject of a future work. A simple approach to infer the endo/exo concentration effect has been obtained from the total amount of neutral or charged species. Therefore, either exo- or endo-fullerenes concentration has been doubled for both neutral or charged species. The Figure 4 shows that an increment in the amount of endofullerenes (endo/exo 2:1) also produces an incre-

ment in the 17.4 μ m/18.9 μ m ratio with respect to the endo/exo 1:1 concentration, while an exofullerenes increment (endo/exo 1:2) reduces such intensity ratio. So, for the same ionization level, different 17.4 μ m/18.9 μ m ratios are obtained depending on the endo/exo concentration. This behavior stressed the marked loss of intensity in the 18.9 μ m feature provoked by metalloendofullerenes. However, the general trend remains to be dominated by the presence of more neutral species against the charged ones. As the level of ionization rises we would expect that the curves corresponding to each circumstellar envelope tend to approximate each other.

4. ASTROPHYSICAL IMPLICATIONS AND CONCLUDING REMARKS

As it was mentioned above, [Brieva et al. \(2016\)](#) have highlighted that the use of C₆₀ relative intrinsic strengths from laboratory data does not explain the large range of 17.4 μ m/18.9 μ m band ratios (~ 0.2 - 1.2) observed in the fullerene-rich circumstellar envelopes around PNe. One possible explanation is the presence of additional emitters contributing to the observed IR spectra. Fullerene-based molecules such as endo(exo)hedral metallofullerenes and fullerene-PAH adducts, among others, are natural candidate species although, to our best knowledge, no additional emitter has been identified to date.

Our DFT calculations and corresponding simulated IR spectra for metallofullerene species reveal that the 17.4 μ m/18.9 μ m band ratio mainly depends on the metal abundances, ionization level, and endo/exo concentration in the circumstellar envelopes. Interestingly, the theoretically predicted 17.4 μ m/18.9 μ m band ratios (~ 0.7 - 1.2) for C₆₀-PNe agree reasonably well with those observed in Galactic and extra-galactic C₆₀-PNe (~ 0.2 - 1.2) ([García-Hernández et al. 2011b](#); [Brieva et al. 2016](#)); the match is quite exceptional for the Large Magellanic Cloud (LMC) PNe (~ 0.7 - 1.1) ([García-Hernández et al.](#)

2011b), which are the C₆₀-PNe with the metal abundances closest to the composition assumed in the construction of the total weighted mixture metallofullerene spectra. The latter is exemplified in Figure 4 by the LMC PNe LMC 48 and LMC 99.

Furthermore, the consistency of our quantum-chemistry calculations goes beyond the C₆₀-PNe and also explains the astonishing anomalous 17.4 μ m/18.9 μ m ratios observed in the chemically peculiar RCB stars. The two known C₆₀-RCBs display a 18.9 μ m feature much weaker than the 17.4 μ m one (García-Hernández et al. 2011a); 17.4 μ m/18.9 μ m ratios of ~ 1.4 and 2.3 are observed in DY Cen and V854 Cen, respectively (Fig. 4). The theoretically predicted 17.4 μ m/18.9 μ m band ratios (~ 1.1 - 2.0) for the peculiar RCB compositions agree very well with the DY Cen observation, while V854 Cen displays a 17.4 μ m/18.9 μ m ratio larger than the predictions. This, however, is in agreement with the spectral analysis of their *Spitzer* spectra, which shows that the 17.4 μ m feature is dominated by C₆₀ emission in DY Cen, while such feature in V854 Cen is a combination of C₆₀ and PAH emission (García-Hernández et al. 2011a). The unusually large 17.4 μ m/18.9 μ m ratios observed in RCBs are naturally explained by a much larger contribution of neutral metallofullerenes, as expected from their lower T_{eff} and weaker UV radiation fields.

In short, we conclude that metallofullerenes are potential emitters contributing to the observed IR spectra in fullerene-rich circumstellar envelopes, providing for the first time an explanation for the fundamental problem of the large range of 17.4 μ m/18.9 μ m band ratios observed.

We emphasize that a perfect spectral match of the simulated metallofullerene IR spectra with the PNe and RCB *Spitzer* spectroscopic observations is not possible. Apart from the four strongest neutral C₆₀ features, there is a no complete one to one correspondence and we cannot discard the presence of others carriers (even other fullerene-based species, see below) affecting the same IR features. However, from our quantum-chemistry calculations it seems clear that the neutral metallofullerenes species significantly contribute to the 6-9 μ m C-C stretching region because of the metal-carbon cage binding effect (see Sect. 3). A similar spectral effect would be thus expected for other fullerene-based neutral species. Indeed, a genuine characteristic

of fullerene-rich PNe environments with unusually high 17.4 μ m/18.9 μ m ratios like the LMC PNe analyzed here (see Fig. 4) is the general presence of a broad and complex (with multiple components/peaks) IR feature at 6-9 μ m (García-Hernández et al. 2012); something that strongly suggest the presence of fullerene-based neutral species such as neutral metallofullerenes, among others.

Finally, we note that most fullerene-rich circumstellar envelopes have been previously observed at low resolution ($R \sim 120$) by *Spitzer*, strongly limiting the detection of the weaker (and more specific) mid-IR features of endo(exo)hedral metallofullerenes (both neutral and charged; see Figs. 1 to 3). Surprisingly, the only two C₆₀-MCPNe observed at higher resolution ($R \sim 600$; ~ 10 - 20 μ m) with *Spitzer* display the presence of new IR emission features not previously observed in astrophysical environments (García-Hernández et al. 2011b). Such new IR emission features are potentially due to specific fullerene-based species such as metallofullerenes; most of them, however, remained as tentative because of the low-quality ($S/N \sim 10$ at the continuum) *Spitzer* spectra (García-Hernández et al. 2011b). The JWST, with a much higher sensitivity (and spectral resolution) than *Spitzer*, has the potential to unambiguously detect the spectral signatures of new IR emission features potentially due to metallofullerenes (or even other fullerene-based species). Thus, high S/N (> 100) and high-resolution ($R \sim 2,400$ on average) JWST spectroscopic observations of fullerene-rich envelopes (e.g., C₆₀ PNe and RCBs) are strongly encouraged in order to confirm or refute the presence of metallofullerenes in circumstellar environments.

5. ACKNOWLEDGMENTS

We acknowledge support from the ACIISI, Gobierno de Canarias, and the European Regional Development Fund (ERDF) under a grant with reference PROID2020010051 as well as the State Research Agency (AEI) of the Spanish Ministry of Science and Innovation (MICINN) under grants PID2020-115758GB-I00 and PID2019-110091GB-I00. This article is based upon work from COST Action NanoSpace, CA21126, supported by COST (European Cooperation in Science and Technology).

APPENDIX

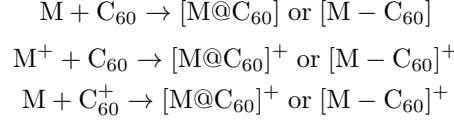
A. WEIGHTED SIMULATED SPECTRA

The IR intensity (I) can be defined as $I \propto (\partial\mu/\partial x)^2$ where $\partial\mu$ stands for the change in the dipole moment and ∂x the displacement produced by the corresponding vibrational mode. Another factor that determines the peak intensity

in the IR is the concentration (n_i) of i molecules or species:

$$I \propto \sum_i^j \left(\frac{\partial \mu}{\partial x} \right)^2 n_i \quad (\text{A1})$$

The summation indicates the contribution from species i^{th} to j^{th} . In our case these species are the metallofullerenes obtained in the reactions between the metal (M) and C_{60} :



We note that the third reaction implying a metal and C_{60}^+ can be discarded because there is no evidence for the presence of C_{60}^+ in the circumstellar environments around PNe and RCB stars (Berné et al. 2013; Cordiner et al. 2019). According to the aforementioned reactions, the metallofullerenes concentration thus depends on the amount of M, M^+ , and C_{60} . From stellar nucleosynthesis models or direct measurements (see below) is possible also to extract the total metal abundances $M_T = M + M^+$, while C_{60} can be estimated as the excess reactant due to the larger abundance of carbon $C \gg M_T$. Fullerene-rich PNe display a narrow T_{eff} range ($\sim 30,000$ - $50,000$ K) and chemical abundances similar to their progenitors; i.e., slightly metal-poor ($Z \sim 0.004$) and low-mass (1.5 - $2.5 M_\odot$) asymptotic giant branch (AGB) stars (Otsuka et al. 2014). We note that our simulated IR spectra do not change significantly for 1.5 - $2.5 M_\odot$, due to the fact that the relative metal abundances remain almost constant in this mass range. Thus, for C_{60} -PNe the metal abundances for a $2 M_\odot$ AGB star were taken from AGB nucleosynthesis models (Karakas 2010; Karakas et al. 2018); note also that not all metals considered here have been directly measured in C_{60} -PNe and we thus need the metal abundance values from theoretical predictions. However, the total metal abundances measurements reported by Jeffery et al. (2011) were used for the only two fullerene-rich RCBs V854 Cen ($T_{eff}=6,750$ K) and DY Cen ($T_{eff}=19,500$ K) (García-Hernández et al. 2011a). Accordingly, M and M^+ are the limiting factors in the metallofullerenes formation. Using the well-know Saha equation (Saha 1920) we are able to predict the concentration of M and M^+ by:

$$\frac{n_{M^+}^2}{n_M} = \frac{G_{M^+} g_e}{G_M} \frac{(2\pi m_e k T)^{3/2}}{h^3} \exp\left(-\frac{IP_1}{k T_{eff}}\right) \quad (\text{A2})$$

with n_{M^+} and n_M being the density of atoms in ionized and neutral states, respectively. The degeneracy of the ionized or neutral state is represented by G_{M^+} or G_M whilst g_e is the electron degeneracy. Finally, T_{eff} is the effective temperature of the PNe/RCB central star, and IP_1 denotes the first ionization potential of the metal; remained variables are the Boltzmann (k) and Planck (h), and the electron mass m_e constants. Applying also $n_{M_T} = n_{M^+} + n_M$ and $\chi = \frac{n_{M^+}}{n_{M_T}}$, where χ indicates the fraction of ionized atoms, we obtain:

$$\frac{\chi^2}{1 - \chi} = \frac{\frac{G_{M^+} g_e}{G_M} \frac{(2\pi m_e k T)^{3/2}}{h^3} \exp\left(-\frac{IP_1}{k T_{eff}}\right)}{n_{M_T}} \quad (\text{A3})$$

From equation A3 we extract n_{M^+} and n_M to weight the intensities according to:

$$I_{M^+} \propto \sum_i^j \left(\frac{\partial \mu}{\partial x} \right)^2 n_{M^+} \quad (\text{A4})$$

$$I_M \propto \sum_i^j \left(\frac{\partial \mu}{\partial x} \right)^2 n_M \quad (\text{A5})$$

$$I_T = I_M + I_{M^+} \quad (\text{A6})$$

The variable I_T is used to construct the total weighted mixture spectra of metallofullerenes and I_M, I_{M^+} the corresponding neutral and charged contributions.

REFERENCES

- Bader, R. 1990, Atoms in Molecules: A Quantum Theory (Oxford: Oxford University Press)
- Becke, A. D. 1993, JChPh, 98, 5648, doi: [10.1063/1.464913](https://doi.org/10.1063/1.464913)

- Berné, O., Mulas, G., & Joblin, C. 2013, *A&A*, 550, L4, doi: [10.1051/0004-6361/201220730](https://doi.org/10.1051/0004-6361/201220730)
- Brieva, A. C., Gredel, R., Jäger, C., Huisken, F., & Henning, T. 2016, *ApJ*, 826, 122, doi: [10.3847/0004-637X/826/2/122](https://doi.org/10.3847/0004-637X/826/2/122)
- Cami, J., Bernard-Salas, J., Peeters, E., & Malek, S. E. 2010, *Sci*, 329, 1180, doi: [10.1126/science.1192035](https://doi.org/10.1126/science.1192035)
- Campbell, E. K., Holz, M., Gerlich, D., & Maier, J. P. 2015, *Nature*, 523, 322, doi: [10.1038/nature14566](https://doi.org/10.1038/nature14566)
- Cordiner, M., Linnartz, H., Cox, N., et al. 2019, *ApJL*, 875, L28, doi: [10.3847/2041-8213/ab14e5](https://doi.org/10.3847/2041-8213/ab14e5)
- Dennington, R., Keith, T. A., & Millam, J. M. 2019, *GaussView Version 6*
- Ditchfield, R., Hehre, W. J., & Pople, J. A. 1971, *JChPh*, 54, 724, doi: [10.1063/1.1674902](https://doi.org/10.1063/1.1674902)
- Dunk, P. W., Adjizian, J. J., Kaiser, N. K., et al. 2013, *PNAS*, 110, 18081, doi: [10.1073/pnas.1315928110](https://doi.org/10.1073/pnas.1315928110)
- Frisch, M. J., Trucks, G. W., Schlegel, H. B., et al. 2016, *Gaussian 16 Revision C.01*
- García-Hernández, D. A., Cataldo, F., & Manchado, A. 2013, *MNRAS*, 434, 415, doi: [10.1093/mnras/stt1032](https://doi.org/10.1093/mnras/stt1032)
- García-Hernández, D. A., Kameswara Rao, N., & Lambert, D. L. 2011a, *ApJ*, 729, 126, doi: [10.1088/0004-637X/729/2/126](https://doi.org/10.1088/0004-637X/729/2/126)
- García-Hernández, D. A., Manchado, A., García-Lario, P., et al. 2010, *ApJL*, 724, L39, doi: [10.1088/2041-8205/724/1/L39](https://doi.org/10.1088/2041-8205/724/1/L39)
- García-Hernández, D. A., Villaver, E., García-Lario, P., et al. 2012, *ApJ*, 760, 107
- García-Hernández, D. A., Iglesias-Groth, S., Acosta-Pulido, J. A., et al. 2011b, *ApJL*, 737, L30, doi: [10.1088/2041-8205/737/2/L30](https://doi.org/10.1088/2041-8205/737/2/L30)
- Jaeger, T. D., van Heijnsbergen, D., Klippenstein, S. J., et al. 2004, *JChS*, 126, 10981, doi: [10.1021/ja0477165](https://doi.org/10.1021/ja0477165)
- Jeffery, C. S., Karakas, A. I., & Saio, H. 2011, *MNRAS*, 414, 3599, doi: [10.1111/j.1365-2966.2011.18667.x](https://doi.org/10.1111/j.1365-2966.2011.18667.x)
- Karakas, A. I. 2010, *MNRAS*, 403, 1413, doi: [10.1111/j.1365-2966.2009.16198.x](https://doi.org/10.1111/j.1365-2966.2009.16198.x)
- Karakas, A. I., Lugaro, M., Carlos, M., et al. 2018, *MNRAS*, 477, 421, doi: [10.1093/mnras/sty625](https://doi.org/10.1093/mnras/sty625)
- Keith, T. A. 2019, *AIMAll* (Version 19.10.12). aim.tkgristmill.com
- Kern, B., Strel'nikov, D., Weis, P., Böttcher, A., & Kappes, M. M. 2013, *JPCA*, 117, 8251, doi: [10.1021/jp4054605](https://doi.org/10.1021/jp4054605)
- Kwok, S. 2016, *A&A Rv*, 24, 8, doi: [10.1007/s00159-016-0093-y](https://doi.org/10.1007/s00159-016-0093-y)
- Lee, C., Yang, W., & Parr, R. G. 1988, *PhRvB*, 37, 785, doi: [10.1103/PhysRevB.37.785](https://doi.org/10.1103/PhysRevB.37.785)
- Otsuka, M., Kemper, F., Cami, J., Peeters, E., & Bernard-Salas, J. 2014, *MNRAS*, 437, 2577, doi: [10.1093/mnras/stt2070](https://doi.org/10.1093/mnras/stt2070)
- Parker, S. F. 2010, *JPCA*, 114, 1657, doi: [10.1021/jp905958b](https://doi.org/10.1021/jp905958b)
- Robledo, M., Aguirre, N. F., Díaz-Tendero, S., Martín, F., & Alcamí, M. 2014, *RSC Adv.*, 4, 53010, doi: [10.1039/C4RA10776D](https://doi.org/10.1039/C4RA10776D)
- Sadjadi, S., Parker, Q. A., Hsia, C.-H., & Zhang, Y. 2022, *ApJ*, 934, 75, doi: [10.3847/1538-4357/ac75d5](https://doi.org/10.3847/1538-4357/ac75d5)
- Saha, M. N. 1920, *Lond. Edinb. Dublin philos. mag. j. sci.*, 40, 472, doi: [10.1080/14786441008636148](https://doi.org/10.1080/14786441008636148)
- Sternberg, A., Hoffmann, T. L., & Pauldrach, A. W. 2003, *ApJ*, 599, 1333
- Szczepanski, J., Wang, H., Vala, M., et al. 2006, *ApJ*, 646, 666, doi: [10.1086/504867](https://doi.org/10.1086/504867)
- Wang, Y., Díaz-Tendero, S., Alcamí, M., & Martín, F. 2017, *JChS*, 139, 1609, doi: [10.1021/jacs.6b11669](https://doi.org/10.1021/jacs.6b11669)
- Zapata Trujillo, J. C., & McKemmish, L. K. 2022, *WIREs Comput. Mol. Sci.*, 12, e1584, doi: <https://doi.org/10.1002/wcms.1584>